Charge-Tunable Autoclaved Silk-Tropoelastin Protein Alloys That Control Neuron Cell Responses

*Xiao Hu, Min D. Tang-Schomer, Wenwen Huang, Xiao-Xia Xia, Anthony S. Weiss, and David L. Kaplan**

Tunable protein composites are important for constructing extracellular matrix mimics of human nerve tissues with control of charge, structural, and mechanical properties. Molecular interaction mechanisms between silk fibroin protein and recombinant human tropoelastin, based on charge, are utilized to generate a new group of multifunctional protein alloys with different net charges. These new biomaterials are then utilized as a biomaterial platform to control neuron cell response. With a +38 net charge in water, tropoelastin molecules provide extraordinary elasticity and selective interactions with cell surface integrins. In contrast, negatively charged silk fibroin protein (net charge −36) provides remarkable toughness and stiffness with morphologic stability in material formats via autoclaving-induced beta-sheet crystal physical crosslinks. The combination of these properties in alloy format extends the versatility of both structural proteins, providing a new biocompatible, biodegradable, and charge-tunable biomaterial platform for neural repair. The data point to these protein alloys as an alternative to commonly used charged synthetic polymers, particularly with regard to the versatility of material formats (e.g., gels, sponges, films, fibers). The results also provide a practical example of physically designed protein materials with control of net charge to direct biological outcomes, in this case for neuronal tissue engineering.

1. Introduction

Neural tissue repair and regeneration strategies are critical since they dealing with complex relationships between components of peripheral and central nervous systems. Therapy for disorders of nervous systems mainly rely on topographical, electrical and chemical cues for the adhesion and proliferation of neural cells. Neural tissue engineering strategies provide an efficient way to better control the microenvironments of cells by implanting artificial extracellular matrixes to promote nerve regeneration and repair of injury and damage. A useful biomaterial for neural tissue engineering should include controllable elasticity and biodegradablility without toxic degradative products, the ability to deliver bioactive factors and drugs for neuron repair, and the most important feature—a matrix to support the extension and electrical activity of neuron cells. Among all of these factors, the most challenging is to design a biomaterial with suitable control of charge density to promote the formation of neural networks and to stimulate cellular differentiation.[1,2] A number of different materials have been explored for aiding nerve regeneration, including the piezoelectric polymer poly(vinylidene fluoride) (PVDF), the electrically conducting polymer poly(pyrrole), poly D,L-lactic-*co*-glycolic acid (PLGA), poly-e-caprolactone (PCL), poly L-lactic acid (PLLA) and poly-L-lysine.[1,2] Although these biomaterials meet some of the needs outlined above, issues of biocompatability, mechanical properties and charge tunability remain as challenges.[1,2]

Therefore, designing new biomaterial systems based on protein composites or alloys is a strategy to control material mechanics, cell interactions, and many related tissue processes and responses. Combinations of silk and recombinant human tropoelastin, two well-established biodegradable proteins with good biocompatibility, can generate new multifunctional protein composite systems that can offer a broad platform of utility to the biomaterials field.[3,4] Human tropoelastin, as the precursor of elastin networks, has extraordinary elastic capacities and can extend multiples of its untensioned length with minimal energy loss, and is a near perfect spring ahead of other natural elastomers and synthetic rubbers.[5–7] Moreover, natural tropoelastin protein is a multifunctional molecule that balances substantial elasticity with the ability to cross-link and selectively interact with cell surface integrins such as $\alpha v\beta 3$ via the C-terminal region and with other matrix proteins such as glycosaminoglycans.[5–8] These are the features that more reductionist bioengineered elastins lack.[9] In contrast, silk fibroin protein is a remarkable fibrous protein with high toughness and stiffness,[10–12] and can provide morphologic versatility in biomaterial formats such as films,[13] sponges,[14] particles,[15] hydrogels,[16] or fibers,[17] and with controllable biodegradation

Prof. X. Hu,[+] Dr. M. D. Tang-Schomer, Dr. W. Huang, Dr. X.-X. Xia, Prof. D. L. Kaplan
Department of Biomedical Engineering
Tufts University
Medford, MA 02155, USA
E-mail: david.kaplan@tufts.edu
Prof. A. S. Weiss
School of Molecular Bioscience
The University of Sydney
Sydney, NSW 2006, Australia
[+] Present address: Department of Physics and Astronomy, Rowan University, Glassboro, NJ 08028, USA

DOI: 10.1002/adfm.201202685

ability.[18] These material features have been widely evaluated in many biomedical systems,[19] as well as biophotonic and bioelectronic systems.[20,21]

In this study, we demonstrate that interaction mechanisms of silk with human tropoelastin were manipulated by net charge attraction, resulting in a unique way to generate net charge-controllable protein alloy biomaterials. In addition, a new crosslinking method based on autoclaving was developed to generate stable silk-elastin alloys with high crystallinity, which eliminates solubility problems with low beta-sheet content found in previous studies, while also providing a simple way to prepare samples for cell culture.[3,4] These results provided a practical method to physically control biological outcomes with neuron cells in elasticity- and charge-tunable protein scaffolds, providing a new strategy for designing biomaterials for neuronal tissue engineering.

2. Results and Discussion

The stabilization of silk-tropoelastin ECM mimics based on chain interactions at the molecular level can be verified via bioinformatics analysis. **Figure 1**a displays the chain interaction analysis between silk and tropoelastin. The amino acids are typically classified as hydrophobic (A, G, L, V, W, C, I, M, F, P), hydrophilic (N, Q, S, T, Y, R, D, E, H, K), positively charged (R and K), and negatively charged (D and E).[15,22,23] Both tropoelastin and silk fibroin showed periodic hydrophobic-hydrophilic domain patterns (Figure 1a and Supporting Information Figure S1b). The hydrophilic domains are often charge-rich, while the hydrophobic domains are composed of repeating sequences of mostly uncharged peptides.[5–8,22] A net charge of +38 was estimated for recombinant tropoelastin at pH 7 based on its amino acid sequence (amino acid residues 27–724 of GenBank entry AAC98394 (gi 182020)) and using standard pKa values for side chain residues (Supporting Information Figure S1a). Two major types of domains are found in tropoelastin chains, hydrophobic repeating domains such as GVGVP and GVGVAP, and hydrophilic domains rich in Lys and Ala (such as AAAKAAKAA) (Figure 1a).[5–8] Other hydrophilic domains do not contain poly-Ala tracts but have Lys near a Pro instead.[5–8] The C-terminus of tropoelastin is highly basic, containing two Cys residues and terminating with a positively charged RKRK sequence, while the N-terminus is a 26-amino-acid signal peptide.[5–8] The unusual highly hydrophilic domain, encoded by exon 26A, is specifically enriched for Ser and charged residues (Glu, Asp, Arg), with the only His in tropoelastin.[5–8] In contrast, the amino acid sequence for silk fibroin has a net charge of −36, estimated at pH 7 in aqueous solution, including a contribution of −29 from the heavy chain and −7 from the light-chain (linked by a single disulfide bond at the carboxyl terminus of H-chain (Cys-c20) and L-chain (Cys-172)) (Figure 1a).[15,22,23] The N- and C-termini of the H-chain are both hydrophilic domains with a negative net charge at the N-terminus and a positive net charge at the C-terminus. The L-chain has a dominant average negative net charge and counterbalanced amphiphilicity. The repetitive part in H-chain consists of long hydrophobic repeating domains such as $(GAGAGS)_n$, blocked with short intervening hydrophilic domains (spacers) with negative charges.[10–15]

The above bioinformatics analysis suggests a suitable match in terms of electrostatic attraction and hydrophobic-hydrophilic interactions between silk and tropoelastin chains. Therefore, the formation of insoluble silk-tropoelastin biomaterials does not require chemical crosslinking, unlike other protein-based materials (e.g., resilins[24] and elastins[25] etc.), due to their strong physical associations by charge in solution, and their beta-sheet crystal networks induced in the solid state.[26,27] This charge-induced interaction between silk and tropoelastin is significantly different from most recombinant block copolymer systems, such as the silk-elastin-like copolymers (SELPs) or variable elastin-like and silk-like multimers.[28–30] These proteins usually focus on charge-intensive repeating units such as $(GAGAGS)_n$ or $(GVGVP)_n$, but not the electrostatic properties of full length natural proteins.[28–30] To elucidate this mechanistic interaction, an interaction model is proposed (Figure 1b). Three types of protein chain interactions are hypothesized to occur at different folding stages: i) Electrostatic interactions first occur between charged amino acid side chains of silk and tropoelastin during solution mixing. According to the bioinformatics analysis (Figure 1a), each tropoelastin chain (+38 net charges) can attract one silk fibroin chain (−36 net charges), from a stoichiometric perspective. This attraction between positive charge sites in tropoelastin and negative charge sites in silk promote initial self-assembly of silk-tropoelastin aggregates in water (Figure 1b). Due to their differences in length, the shorter tropoelastin chains (60 kDa) could dominate an inner layer, surrounded by the longer silk chains (≈420 kDa). This assumption was shown based on our prior AFM studies,[3] with nanoporous structures observed on silk-tropoelastin films when the molar ratio of silk to tropoelastin was ≈1 (e.g., sample SE90 in the previous and present study).[3] Nanopore dimensions were calculated with long axis close to 26 nm ± 4 nm and short axis around 17 nm ± 4 nm, with a long axis/short axis ratio of 0.68 ± 0.2. This result is close to the theoretical size of tropoelastin dimers/monomer, which has a typical size of ≈20 nm along its length, 16 nm end-to-end measured by small angle X-ray and neutron scattering in solution, with the ratio of the thickest axis 7.5 nm to the long ≈11 nm side around 0.68.[31] Protein sequences with dominate hydrophobic (non polar) side chains may be packed on the surface of the primary silk-tropoelastin aggregates to protect the interior hydrophilic (polar) cores, so that the protein aggregates assemble with the lowest surface energy when interacting with a water environment. Similar structures have been found in silk fibroin particles[12,15] and elastin-like $(VPGVG)_2(VPGEG)(VPGVG)_{215}$ polypeptide.[32] ii) In addition, the hydrophobic-hydrophilic interactions between silk-tropoelastin protein chains and the electrostatic force between primary silk-tropoelastin aggregates direct the formation of larger protein aggregates in water. This prediction was also confirmed by AFM[32] where a widely distributed multi-micelle aggregate structure with diameter of 1–2 μm was found on the surface of cast 0.02 wt% silk-tropoelastin solutions when the molar ratio of silk to tropoelastin was ≈1 (as an example, three large aggregates from sample SE90 are evident in the right side of the large aggregate model in Figure 1b). Furthermore, with increasing tropoelastin in the solution (e.g., SE75, SE50, SE25, SE10 in this study), hydrophobic interactions could also occur between pure tropoelastin chains and with silk-tropoelastin aggregates, resulting

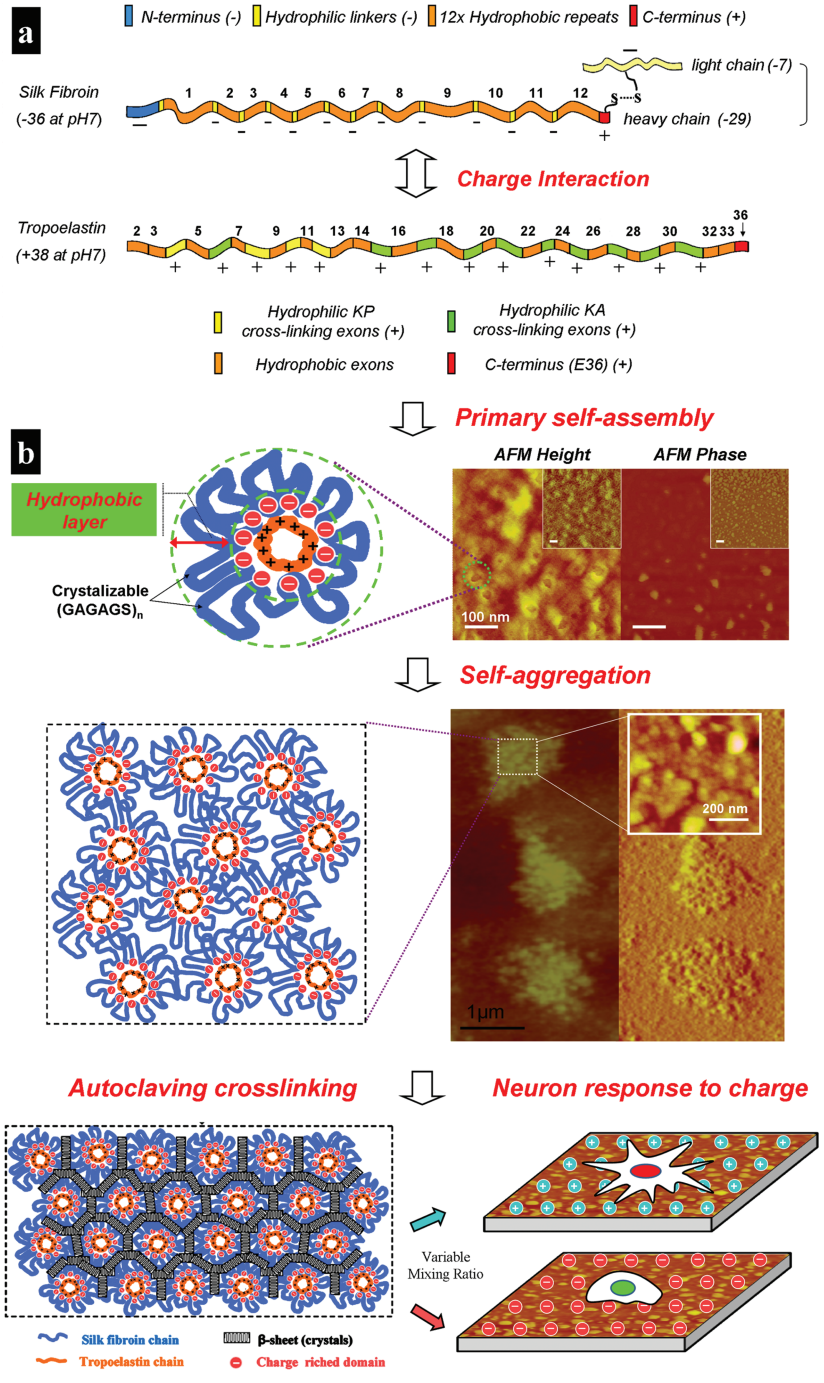

Figure 1. a) Bioinformatics analysis of silk fibroin and human tropoelastin protein chains. Both silk and tropoelastin sequences have repetitive hydrophobic and hydrophilic domains, and the length of tropoelastin (60 kDa, lacking the signal sequence encoded by exon 1) is shorter than that of silk chains (≈420 kDa). However, from the view of net charges in their side chain groups, each tropoelastin chain (+38 net charge) can attract nearly one silk fibroin chain (–36 net charge) at pH 7 aqueous solution. b) Primary self-assembly, aggregation, and crosslinking model of silk-tropoelastin materials. The charged amino acid side chain groups of silk and tropoelastin first interact with each other and form primary aggregates (≈200 nm) during solution mixing. Then the primary aggregates associate to form larger aggregates around 1–2 μm. During energy input such as physical autoclaving process, the different silk-tropoelastin films can be physically crosslinked by beta-sheet crystals and form insoluble materials with variable charges on their surfaces, related to the subsequent neural cell studies.

in complicated aggregates (r > 50 nm) that are similar to large silk-tropoelastin aggregates yet several times larger than the tropoelastin monomers (r ≈ 6 nm), also supported by AFM and DLS (Supporting Information Figure S2). iii) Finally, beta-sheet structures related to hydrogen bonds can be formed between the silk-tropoelastin aggregates during energy input, such as heating in water. This process is irreversible due to the formation of beta-sheet crystals.[10–13,33] For the silk-tropoelastin films, protein aggregates collapse during drying, during additional thermal treatment such as autoclaving in this study[34] or during annealing in water vapor as we have previously reported.[13] This effect will result in an insoluble beta-sheet crystal network (Figure 1b), which can physically crosslink the films to allow stability such as during cell culture and related physiological environments.

The size distribution of the silk-tropoelastin aggregates was further characterized by dynamic light scattering (DLS). Supporting Information Figure S2 shows the hydrodynamic radius (Rh) vs. intensity distribution of all silk-tropoelastin samples in 0.1-wt% solution (SE0, SE10, SE25, SE50, SE75, SE90, and SE100). Notably, scattered light at a hydrodynamic radius (Rh) of around 6 nm with a predicted molecular weight of 59 kDa ± 12 kDa for sample SE0 is due to pure tropoelastin monomers in solution, as previously reported.[35,36] In contrast, pure silk (SE100) showed strong intensity of scattered light at Rh of 57.1 nm ± 9.1 nm and a predicted molecular weight of 427 kDa ± 84 kDa, indicating that silk monomers and some small silk aggregates were formed in solution.[12,22] After 10 wt% of tropoelastin was added into the silk solution (SE90), the Rh of major aggregates in solution significantly increased to 404.5 nm ± 126.9 nm, with only <3% intensity distribution at 43.5 nm ± 4.1 nm. This effect is predictable since the molar ratio for silk/tropoelastin in SE90 is 56.5/43.5 (with a net charge of –03.8), suggesting neutral silk-tropoelastin aggregates are dominate in the solution. In addition, the silk-tropoelastin aggregates in SE90 were collected by centrifugation, and their zeta-potential at pH 7 determined. A neutral potential of –0.33 mV ± 1.56 mV was obtained, compared with –43.5 mV ± 2.5 mV from pure silk micro-particles.[15] An increase in tropoelastin content in samples SE75 and SE50 increased the intensity of scattered light to around 5–10 nm, while the radius distribution for the large silk-tropoelastin aggregates (around 350–550 nm) remained stable. These results indicated that many abundant free tropoelastin chains had assembled into small

aggregates themselves or with silk residues in solution. When tropoelastin began to dominate in SE25, SE10, the large silk-tropoelastin aggregates became more complex and the size distribution broadened above 1 μm. There was a notable amount of free tropoelastin chains around 5 nm. Collectively, the results point to an important role of the silk to tropoelastin ratio in self-assembly and size of silk-tropoelstin aggregates.

To examine the transitions of the silk-tropoelastin aggregates, temperature-dependent CD scans were performed from 5 °C to 95 °C, and then cooled back to 5 °C for each silk-tropoelastin solution. **Figure 2**a illustrates heating scans for SE100, SE90, SE75, SE50, SE25, and SE0, with the initial 5 °C scans as blue lines and the final 95 °C scans as red lines. For the tropoelastin-dominated samples (SE25 or SE10), structural transitions were similar to that of pure tropoelastin (SE0), which showed a typical disordered protein coacervation (increase at 200 nm with a stable shoulder near 220–225 nm) with increase of temperature.[35,36] The charge effects in the protein composite system were not strong in these samples. However, upon addition of more silk (SE90, SE75, SE50), the interaction between silk and tropoelastin became significant. This was demonstrated in the solution of SE75, in which beta-sheet structures (≈215 nm) and helix structures (≈209 nm and 222 nm) gradually formed with increasing temperature. This finding also indicated that strong transitions only occurred in the silk mass-dominated composite samples with close charge interactions, while pure silk fibroin protein (SE100, Figure 2a) did not transitions in water in this temperature region. Therefore, charge-induced silk-tropoelastin aggregates in SE90, SE75, and SE50 were stable and could be used to induce irreversible beta-sheet crystallization during thermal transitions. In contrast, charge impacts on SE25 or SE10 are not obvious. We elected not to continue with these tropoelastin mass-dominated samples, only using pure tropoelastin (SE0) as a control.

Autoclaving is typically used to confer a combination of high temperature (121 °C), steam and high pressure (20 psi) to sterilize materials. We utilized this approach to crosslink the cast silk-tropoelastin films. Figure 2b shows the typical FTIR spectra of different silk-tropoelastin films after autoclaving to induce the crosslinking process, with a) AC-SE0, b) AC-SE50, c) AC-SE75, d) AC-SE90, and e) AC-SE100. Initially, all untreated samples were in the non-crystalline state without peaks in the main wavenumber region of beta-sheet crystal (1600–1640 cm^{-1}), as we have

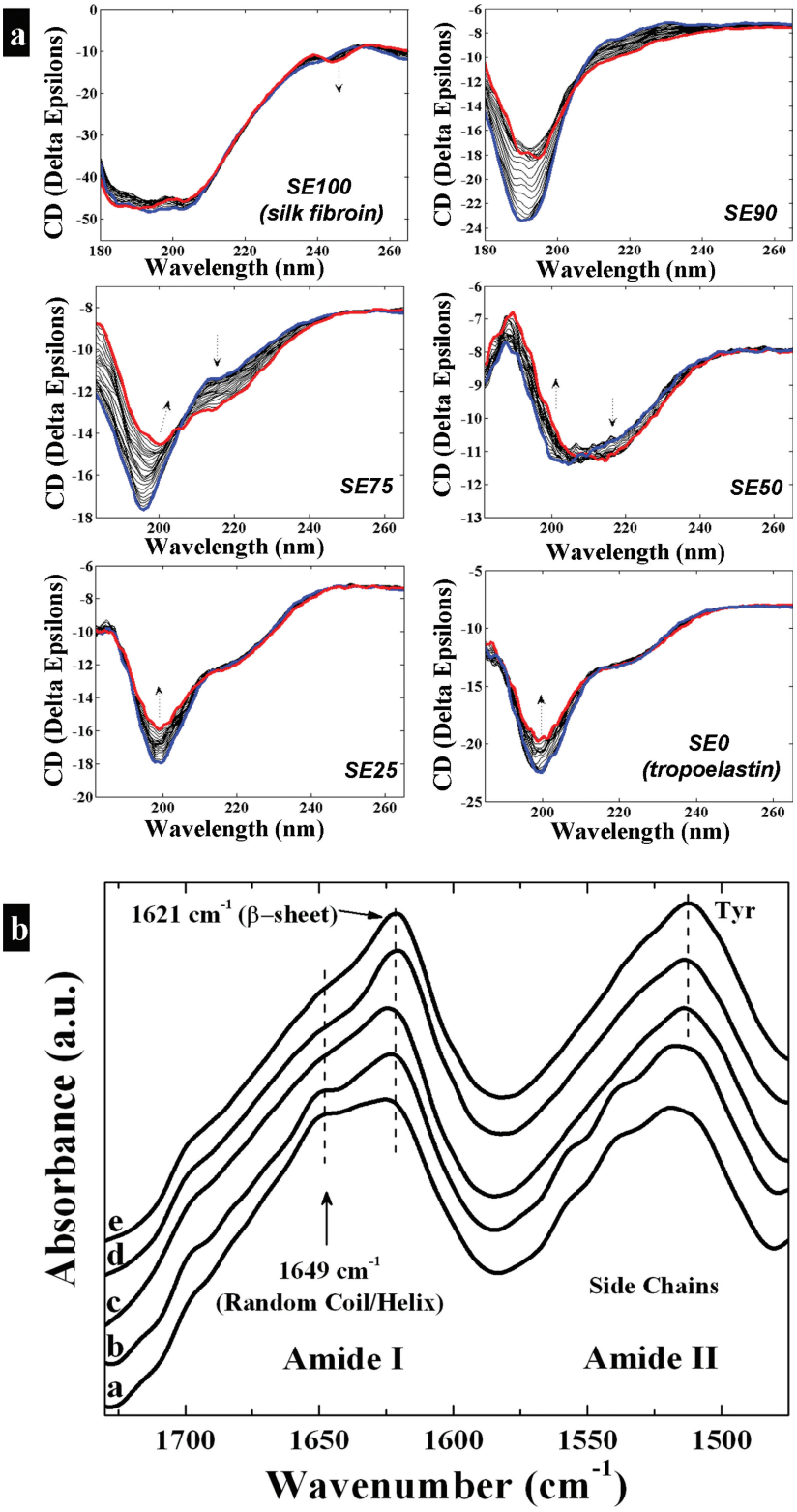

Figure 2. a) Temperature-dependent circular dichroism (CD) scans for 0.02 wt% solutions of SE100, SE90, SE75, SE50, SE25, and SE0. Scans were performed from 5 °C to 95 °C, with initial 5 °C scans as blue lines and final 95 °C scans as red lines in the figure. b) Amide I and II regions of typical FTIR spectra of different silk-tropoelastin films after the autoclaving crosslinking process for curves: a) AC-SE0, b) AC-SE50, c) AC-SE75, d) AC-SE90, and e) AC-SE100. After treatment, the beta-sheet crystal peak appeared in all samples, centered at 1621 cm^{-1}.

Table 1. Mass and molar ratios, tensile-stress test results (elastic modulus and elongation ratios), and calculated beta-sheet crystallinities of autoclaving crosslinked silk-tropoelastin films.

Sample	Mass ratio [Silk/Tropoelastin]	Elastic Modulus [MPa]	Molar ratio [Silk/Tropoelastin]	Net Charge at pH 7.4 (or pH 7.0)	Elasticity (Elongation) [%]	Beta-shee Crystallinity [%]
AC-SE100	100/0	68.5 ± 4.3	100/0	−36.1 (−34.6)	23.5 ± 9.0	59.2 ± 1.3
AC-SE90	90/10	53.9 ± 2.2	56.3/43.7	−03.8 (−02.9)	56.2 ± 6.5	57.3 ± 1.4
AC-SE75	75/25	33.0 ± 3.6	30.0/70.0	+15.6 (+16.1)	28.7 ± 2.6	56.6 ± 0.9
AC-SE50	50/50	26.2 ± 4.0	12.5/87.5	+28.5 (+28.8)	25.1 ± 8.2	53.8 ± 0.8
AC-SE0	0/100	5.2 ± 1.3	0/100	+37.7 (+37.9)	25.0 ± 4.6	43.6 ± 0.6

Calculated molecular weights: full length silk fibroin is 419 330Da, recombinant human tropoelastin is 59 988 Da. The mass ratio for absolute neutral zero charge at pH 7.4 is 87.97/12.03.

described previously.[3,4] After autoclaving, the beta-sheet crystal peak appeared in all samples, centered at 1621 cm^{-1}, while the random coil peaks (1640–1649 cm^{-1}) and the alpha-helix peak (centered at 1650 cm^{-1}) decreased (Figure 2b). A previously well-developed deconvolution method based on Fourier self-deconvolution (FSD) and Gaussian curve fitting in Amide I region, was then used to calculate the percentage of beta-sheet crystals in the autoclaved samples.[3,13,26] **Table 1** summarizes the percentage of beta-sheets in the different autoclaved silk-tropoelastin samples. Although there was an increase in silk content from AC-SE50 to AC-SE100, the amount of beta sheet was generally similar, with AC-SE50 ≈ 54%, AC-SE75 ≈ 57%, AC-SE90 ≈ 57%, and AC-SE100 ≈ 59%. Previously, we have reported that autoclaving induced the highest beta-sheet crystal fraction observed so far in the pure silk materials (≈60%) such as in scaffolds[34] and films.[37] This effect is due to the dominant $(GAGAGS)_n$ repeating sequence in silk chains that can give beta-sheet structures during energy input.[10,27] However, this is the first report to show that tropoelastin can form up to ≈44% beta sheet structure in films upon autoclaving, which is significantly higher than that in untreated pure tropoelastin films (less than 23% beta sheet).[4,5] In addition, this amount of beta-sheet can maintain tropoelastin films in a stable insoluble shape when soaked in PBS solution. Autoclaved tropoelastin films did not shrink into a fiber-like morphology in solution, in contrast to the water-annealed or methanol-induced physically crosslinked tropoelastin samples reported previously.[4,5] To understand the stability of autoclaved-induced secondary structures in silk-tropoelastin films, samples were also autoclaved for longer times (e.g., autoclaved twice for a total of 50 min, and a third time for a total of 75 min), and then analyzed using FTIR. The results confirmed that longer autoclaving time did not induce additional beta-sheet content in the silk-tropoelastin materials.

Untreated and autoclaved samples were studied by 2D X-ray diffraction to further investigate whether the beta-sheet structure in silk-tropoelastin matrices were similar among the various samples. The results showed that pure silk and pure tropoelastin (**Figure 3**a), as well as all other silk-tropoelastin samples were initially noncrystalline before autoclaving. Only distinct non-crystalline halo peaks were found in their diffraction patterns (Figure 3b,A,B). After autoclaving, crystalline peaks appeared in all samples (Figure 3a,b), with the major peak position slightly moving from 43 nm in AC-SE0 to 47 nm in AC-SE100. Previously, we reported that anti-parallel beta-sheet crystals in silk fibroin films have typical Miller indices of (020)/(200),[27] which are identical to the peak positions displayed in autoclaved AC-SE100 (Figure 3b,G). The shift of beta-sheet peaks in tropoelastin (AC-SE0, Figure 3b,C) may indicate a different packing and morphology for the beta-sheet crystals formed in tropoelastin (e.g., silk I-like crystals).[27] The shape of 3D tropoelastin in solution,[31] reveals that tropoelastin monomers assemble in a specific head-to-tail tandem manner.[31] This multimer interaction could result in differences between the beta-sheet crystals induced in tropoelastin vs. in silk proteins.

Relying on the strong beta-sheet crystal network in the structure, the mechanical properties of physically crosslinked silk-tropoelastin samples were evaluated at 37 °C in a PBS hydrated environment. Figure 3c shows the representative tensile stress/strain curves for the autoclaved silk-tropoelastin films AC-SE100, AC-SE90, AC-SE75 and AC-SE50, and AC-SE0 as a control. The samples exhibited variable force vs. axial strain profiles with changes in silk content. In general, increasing the tropoelastin fraction in films tended to soften the material, resulting in a lower strain value at a defined stress force. This result was expected as tropoelastin molecules confer a reduced rigidity on the extracellular matrix in soft tissues such as skin and vasculature.[6–8,38] This elastic function of tropoelastin is unique in these samples, since the AC-SE100 has a similar content of beta-sheet to the samples AC-SE90, AC-SE75, and AC-SE50 (Table 1). However, tropoelastin-dominated samples such as AC-SE0 may take advantage of both elastic mechanisms of tropoelastin molecules and low beta-sheet crystallinity (≈44%) to enhance film softness. The data in Figure 3d revealed that autoclaved silk films exhibit a significantly ($p^{**} < 0.01$) increased Young's modulus (≈69 MPa) when compared with autoclaved tropoelastin films (≈5 MPa) (Table 1), in addition to their ultimate tensile strength (Figure 3f) and yield stress (Figure 3g). These results also indicated that at least 1–5 MPa Young's modulus was necessary to maintain the original shape of protein bulk films (30–40 μm) for advanced material applications. This is one of the reasons that we did not obtain shape-stable tropoelastin films by other physical crosslinking methods such as water-vapor annealing,[5] which can only generate around 0.5 MPa modulus. However, the sample AC-SE90 showed an unexpectedly higher ($p^{*} < 0.05$) elongation ratio (≈55%) than all other samples including autoclaved pure silk and pure tropoelastin (≈25%) (Figure 3e). This effect is expected for a model

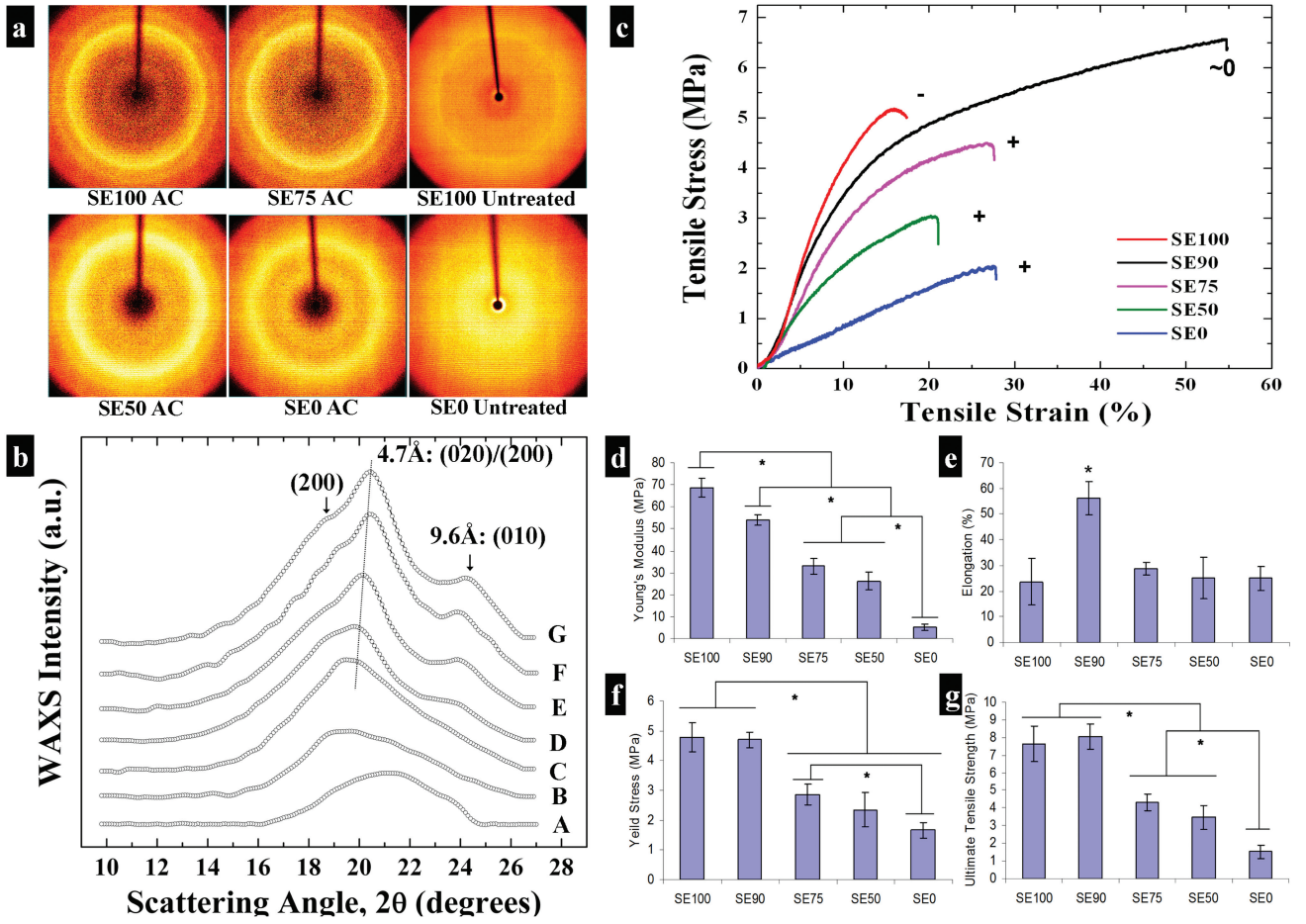

Figure 3. a) 2D X-ray diffraction patterns of untreated and autoclaved silk-tropoelastin films. b) Integral one-dimensional WAXS patterns of these samples to identify crystal peak positions, as A) untreated silk, B) untreated tropoelastin, C) autoclaved (AC)-SE0, D) AC-SE50, E) AC-SE75, F) AC-SE90, and G) AC-SE100. c) Representative tensile stress/strain curves for the AC silk-tropoelastin films SE100, SE90, SE75, SE50, with SE0 as a control at 37 °C PBS solution and their calculated d) modulus of elasticity (Young's modulus), e) elongation ratio (percentage of elasticity), f) yield stress, and g) ultimate tensile strength.

where a neutral charge network in water dramatically improves the stability of the material during mechanical stress or deformation, and might provide an important avenue towards designing and building upon the durability of these and other protein alloys in the future.

Charge variation on extracellular matrices is critical in tuning cell growth and functions such as proliferation, migration, and differentiation, particularly for charge-sensitive neural cells in the brain, spinal cord, and peripheral ganglia.[39–44] Therefore, rat brain cortical neurons were used as a template to understand how net charge modulated neuronal responses to the material interface of silk-tropoelastin protein composites during 2 week in vitro. Previously, we considered how the surface morphology (such as surface roughness and nano/micro scale surface patterns) can induce various responses by human bone marrow derived mesenchymal cells (hMSCs) and C2C12 muscle cells.[4] To eliminate the potential impact of surface morphology on neurons in this study, we first pressed all autoclaved silk-tropoelastin films with polished stainless steel disks by adapting a high pressure pumping system. Surface scans by AFM demonstrated that the pressed silk-tropoelastin films displayed a similar surface roughness around 15–25 nm. FTIR analysis also showed no structural change as a result of this process. The same-sized samples were transferred into 96-well tissue culture plates and allowed to adhere in PBS solution. Low-concentration coated PLL plate surfaces were also used as controls, to establish a positively charged molecular layer which enabled the adhesion of negatively charged cell surfaces. Previously, most neuronal cultures studied on biopolymers relied on this additional coating of PLL.[42,43] There have been effects to identify alternative biomaterials to this positively charged polymer. However, most of these options remain synthetic polymers with concerns for toxicity in vivo.[43] Here, we directly used silk-tropoelastin protein matrices without PLL coatings to examine their charge functions, and to evaluate whether silk-tropoelastin materials, as natural biocompatible protein matrices, can replicate the charge function of PLL coatings. **Figure 4**a demonstrated cell viability of primary cortical neurons from embryonic day 18 (E18) rats on the different silk-tropoelastin alloys during 2, 4, 7, 10 days in vitro (DIV), for the

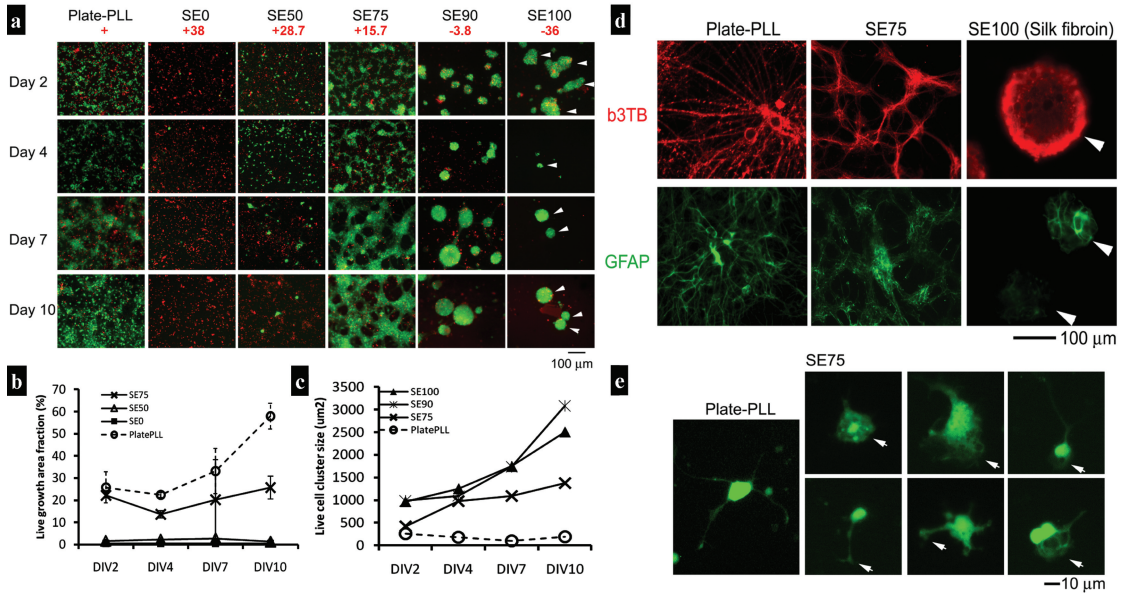

Figure 4. a) Fluorescence images of cell viability assay of primary cortical neuronal cultures (E18) on autoclaved (AC) protein alloy films (SE0, SE50, SE75, SE90, SE100) in comparison to control (Plate-PLL) at different mixing ratios over days in vitro (DIV) (green, live cells; red, dead cells). With little adhesion to silk fibroin, neurons formed clusters (arrowhead). Increasing the tropoelastin content resulted in more adhesion by neurons to the surface; however, a high percentage of tropoelastin led to cell death. Scale bar 100 µm. b) Time-dependent changes in live growth area of neuronal cultures on films of SE75, SE50, SE0 (solid line) in comparison to control (Plate-PLL, dotted line). c) Time-dependent changes in live cell cluster sizes of neuronal cultures on films SE90, SE75, and SE100 (solid line) compared to control (Plate-PLL, dotted line). d) Fluorescence images of immune-stained primary cortical neuronal cultures (E18) on SE75 and pure silk films compared with PLL control plate at day 10 in vitro. Sample SE75 promoted the development of normal neuronal processes, shown immune-stained with β III tubulin (b3TB, red), and development of glial cell morphology, immune-stained with glial fibrillary acidic protein (GFAP, green), similar to PLL. Pure silk fibroin (SE100) resulted in the aggregation of neuronal cells as clusters (arrowhead) that loosely rested on the surfaces. Scale bar 100 µm. e) Fluorescence images of individual live neuronal cells that were stained with calcein AM (green) at early days in vitro (DIV 2–4). Cells on SE75 films showed significantly extended surface contact with the substrate (arrow) compared to the control (Plate-PLL). Scale bar 10 µm.

autoclaved samples AC-SE0, AC-SE50, AC-SE75, AC-SE90, and AC-SE100. Surface charges changed gradually from AC-SE100 (–36) to near neutral AC-SE90 (–3.8), then increasingly positive for AC-SE75 (+15.6), AC-SE50 (+28.5) and AC-SE0 (+37.7). On the control plates of PLL (MW 70 to 150 kDa, with an estimated +20 charge density on the surface after coating procedure), live neurons (green color) readily attached to the PLL surface from day 1, then initiated extensions on day 2, and finally formed an extensive neuronal network after 1 week. In contrast, neurons showed little adhesion to films of pure silk fibroin (AC-SE100) due to the strong negative charge on silk surface (–36); in this case neurons responded by forming clusters that loosely rested on substrate without forming network connections. Increasing the mass ratio of tropoelastin to 10% (AC-SE90), however, resulted in fewer clusters, more surface adhesion and neuronal growth. Near neutral charge surface of AC-SE90 was not the premium condition for the growth of neurons. The sample AC-SE75 with a weak positive charge (+15.6) provided the best neuronal growth environment in the group of silk-tropoelastin matrix, based on the appearance of a tightly connected neuronal network similar to the PLL surface that was observed after 10 days. In contrast, although AC-SE50 had significant neuronal attachment early (days 1 to 4) in culture, the majority of the neuronal cells were dead (red color) by day 7. Similarly, most of the cells on strongly positively charged AC-SE0 films (+37.7) attached to the substrates easily the first day, but then quickly died on day 2. Quantification of live cell growth areas showed that AC-SE75 had a growth trend closer to that of the control of PLL-coated plate (Figure 4b). In addition, cells formed much smaller sized clusters on AC-SE75 films compared to the samples of AC-SE90 and AC-SE100, though still a little larger than those on PLL control plates (Figure 4c). The different responses of the neuron cells on silk-tropoelastin films indicated that substrate net charge regulates the neuronal adhesion and growth on these biomaterial alloys. Several biological factors play a role in this process. Neurons are highly sensitive to external ionic environments particularly Na+ and K+ fluxes. In addition, membrane charge can facilitate interactions with these biomaterial substrates, leading to unknown downstream signaling impact.

After 10 days of growth, immunostaining of neuronal cultures was performed to examine cell morphology for AC-SE100 (silk), AC-SE75, and PLL controls (Figure 4d). Two different cell markers, β-III tubulin (b3TB, red) for neurons, and glial fibrillary acidic protein (GFAP, green) for glial cells, were used and the results showed that both cell types developed well after 10 days with extensive cellular processes and cell-cell connections on the silk-elastin samples, especially on AC-SE75 (Figure 4d). The morphology of cells on AC-SE75 was similar to that of normal and mature cells on PLL control plates. Notably, at early days in vitro (DIV 2–4), individual live neuronal cells displayed spreading and enlarged growth cones on AC-SE75

(Figure 4e), similar to the extended cells growing on PLL control plates. These results revealed that AC-SE75 with weak positive charge can replace PLL coating in future material applications.

3. Conclusions

In summary, the mechanism by which silk fibroin interacts with human tropoelastin was revealed to be net charge attraction and hydrophobic-hydrophilic interactions, that depended on the two types of proteins at different ratios. This type of positive-negative charge interaction induced stable silk-tropoelastin aggregates at the micrometer-scale that transformed to beta-sheet crystals following energy input. A strong physical crosslinking method, autoclaving, was used to prepare insoluble silk-tropoelastin alloys with similar high beta-sheet crystallinity (54% to 59% from AC-SE50 to AC-SE100), yet with different net charges (+28.5 to −36.1 for AC-SE50 to AC-SE100). With increasing tropoelastin content (from AC-SE100 to AC-SE0)), the elastic modulus of silk-tropoelastin alloys decreased gradually with stable solid material formats, which could be used to produce other complex 3D silk-tropoelastin biomaterials (such as hydrogels, nanofibers, or scaffolds). Interestingly, near neutral charge in AC-SE90 provided the highest elasticity (elongation ratio) of the alloys, indicating that the impact of charge interaction is critical in manipulating mechanical functions. In addition, rat cortical neurons were assessed for neuronal network formation and cell viability on the protein films with different net charges during 10 days in vitro. A weak positive surface charge surface, such as AC-SE75 (+16), facilitated stable neuron network formation with longer term viability, similar to PLL coating surface commonly used in most neuron-related biomaterial applications. These significantly different neuron cell responses indicated that silk-tropoelastin protein alloys can regulate growth and formation of charge-sensitive cell networks and tissues with controllable structural and mechanical properties, indicating the specific value of these protein alloy materials in applied cell biology.

4. Experimental Section

Materials: The preparation of silk fibroin and tropoelastin solutions has been reported previously.[3,4] In brief, *Bombyx mori* silkworm cocoons were boiled in a 0.02 M Na_2CO_3 solution to remove sericin proteins. The remaining silk fibroin fibers were dissolved in a 9.3 M LiBr solution at 60 °C for 4 h, and then dialyzed against distilled water in dialysis cassettes for at least 2 days to completely remove LiBr. Finally, a pure 6–8 wt-% silk fibroin aqueous solution was obtained after centrifugation and purification. Recombinant human tropoelastin isoform SHELΔ26A (Synthetic Human Elastin without domain 26A) was prepared and purified from bacteria on a multi-gram scale, as described previously.[3,4] The amino acid sequence of the 60 kDa full-length human tropoelastin protein is same as the amino acid residues 27–724 of GenBank entry AAC98394 (gi 182020). Tropoelastin was then dissolved in distilled water at 4 °C (1 wt%) and slowly mixed with diluted 1 wt% silk aqueous solution to avoid protein gelation. The final 1 wt% blended solutions were based on a mass ratio of silk:tropoelastin = 100:0 (SE100, pure silk) 90:10 (SE90), 75:25 (SE75), 50:50 (SE50), 25:75 (SE25), 10:90 (SE10), and 0:100 (SE0, pure tropoelastin).[3,4] Films were obtained by casting solutions on polydimethylsiloxane (PDMS) substrates to ~30 μm thickness and then stored at 4 °C.

Physical Crosslinking by Autoclaving: Silk-tropoelastin films (30 μm thick) were placed in a polished aluminum dish and sealed into a standard 12 inch × 18 inch Fisherbrand Instant Sealing Sterilization Pouches for autoclaving. Films were steam sterilized by autoclaving under standard condition (T = 121°C, P = 15 psi, t = 25 min), and were named based on the initial mass ratio of silk to tropoelastin: AC-SE100 (pure autoclaved silk), AC-SE90, AC-SE75, AC-SE50, AC-SE25, AC-SE10, and AC-SE0 (pure autoclaved tropoelastin).

Circular Dichroism (CD): CD spectra of silk-tropoelastin solutions (0.02 wt%) were recorded on an Aviv model 62DS spectrophotometer equipped with a Peltier temperature controller (AVIV Biomedical, Inc., Lakewood, NJ) using sandwich quartz cell cuvettes with a 1 mm path length (Nova Biotech, El Cajon, CA). Protein solutions were equilibrated at 4 °C for 20 min before measurements. Temperature-dependent CD scans were performed by increasing from 5 °C to 95 °C and then decreasing from 95 °C to 5 °C with 10 min equilibration at each temperature. Spectra were obtained from 260 to 180 nm at a resolution of 0.5 nm. CD spectra represented the average of three measurements and were smoothed using SigmaPlot data smoothing software. CD data were reported as mean residue ellipticity (θ, deg cm^2 dmol^{-1}).

Dynamic Light Scattering (DLS): DLS was carried out on a DynaPro Titan instrument (Wyatt Technology, Santa Barbara, CA) equipped with a temperature controller. All samples were passed through a 2 μm filter before measurements. The silk-tropoelastin solutions (0.1 wt%) were placed in quartz cuvettes and stabilized at 5 °C for 10 min prior to measurement. Measurements were performed at 5 °C to avoid structural changes at higher temperature. To obtain hydrodynamic radii, the intensity autocorrelation functions were analyzed using the Dynamics software (Wyatt Technology, Santa Barbara, CA).

Zeta Potential Analysis: Zeta potential measurements were performed using a Nanoseries Malvern Zetasizer (Malvern, Worcestershire, UK). Data are based on average values from more than 60 measurements at 5 °C.

Atomic Force Microscopy (AFM): AFM was performed in tapping mode using a Dimension 3100 Scanning Probe Microscope with Nanoscope III and IV controllers (Digital Instruments, Santa Barbara, CA) and equipped with rotated tapping-mode etched silicon probes (RTESP; Nanodevices, Santa Barbara, CA). The silicon tip probe had a spring constant of 1–5 N m^{-1} and a resonance frequency of 60–100 kHz. All samples were cast on mica surfaces and allowed to dry for 2 days. Topography and phase signal images were recorded with 512 × 512 data points.

Fourier Transform Infrared Spectroscopy (FTIR): Infrared spectroscopy of the autoclaved silk-tropoelastin films was performed with a Jasco FT/IR-6200 Spectrometer, equipped with a deuterated triglycine sulfate detector and a horizontal MIRacle ATR attachment fitted with a Ge crystal (Pike Tech., Madison, WI). Each measurement incorporated 128 scans from 600 to 4000 cm^{-1} that were Fourier transformed using a Genzel-Happ apodization function to yield spectra with a nominal resolution of 4 cm^{-1}. To deconvolute spectra with better peak resolution for identifying secondary structures of protein samples and obtain peak positions for the Amide I region (1595 to 1705 cm^{-1}), Fourier self-deconvolution (FSD) was performed using Opus 5.5 software (Bruker Optics Corp., Billerica MA).[3,4] Each peak was assigned to secondary structures:[3,4] absorption bands in the frequency range of 1610 to 1635 cm^{-1} represented β-sheet structure (B); bands around 1640 to 1650 cm^{-1} represented random-coil (R), bands in the range of 1650 to 1660 cm^{-1} were assigned to alpha-helix (A), and peaks above 1660 cm^{-1} were ascribed to β-turn structures (T).[3] Finally, the deconvoluted Amide I spectra were curve-fitted, and area ratios of the above assigned bands to the total Amide I area were used to determine the fraction of the secondary structural contents in the silk-tropoelastin films.

Wide Angle X-Ray Diffraction (WAXD): Autoclaved silk-tropoelastin films about 30 μm in thickness were mounted in a Bruker GADDS D8 X-ray diffractometer (wavelength λ = 0.154 nm) operating at 40 kV and 20 mA. The scattering angle 2θ was first calibrated by silicon reference standard with silicon (111) peak at 28.444°. Each sample was then scanned for 1800 s to obtain a clear diffraction pattern, with a scattering angle that ranged from 4° to 30°. To obtain crystal peak positions and

identify the crystalline content, the 2D WAXS patterns were converted to a one-dimensional pattern by integrating with χ over all sectors (but avoiding the beam stop region). The baseline was determined by subtracting the air background and fitted using quadratic baseline as we described previously.[5]

Mechanical Tests: Uniaxial tensile tests were performed on an Instron 3366 (Norwood, MA, USA) testing frame equipped with a 100 N capacity load cell and Biopuls pneumatic clamps. Autoclaved rectangular shape silk-tropoelastin films (5 mm × 4 cm) were hydrated in 0.1 M phosphate-buffered saline (PBS) for 12 h to reach a swelling equilibrium prior to testing. Test samples were submerged in the temperature-controlled testing container filled with 37 °C PBS. A displacement control mode with a crosshead displacement rate of 5 mm min^{-1} was used with a gauge length of 15 mm. The initial elastic modulus, elongation ratio, yield stress, and ultimate tensile strength were calculated from stress/strain plots. The elastic modulus was calculated by using a least-squares fitting between 0.05 N load and 5% strain past this initial load point. The elongation to failure ratio was determined as the last data point before a >10% decrease in load (failure strain minus the strain corresponding to 0.05 N load noted earlier). The yield strength was determined by offsetting the least-squares line by 2% strain and finding the data intercept. Tensile strength was defined as the highest stress value attained during the test. Each sample set (n = 6) was statistically analyzed by Student t-tests.

Primary Cortical Neuronal Culture: Primary cortical neurons from embryonic day 18 (E18) Sprague Dawley rats (Charles River, Wilmington, MA, USA) were plated on 96-well plates with autoclaved silk-tropoelastin protein films (≈30 μm thickness), and the control wells were coated with 20 ng/mL poly-L-lysine (Sigma-Aldrich, St. Louis, MO, USA) (n = 8 for each condition). Brain tissues were collected in Dr. Steve Moss's laboratory at Center for Neuroscience Research of Tufts University. 200 000 cells were plated per well (625 000 cells/cm^2) then cultured in NeuroBasal media (Invitrogen, Carlsbad, CA, USA) supplemented with B-27 neural supplement, penicillin/streptomycin (100 U/mL and 100 μg/mL), and GlutaMax (2 mM) (Invitrogen). Cells were cultured at 37 °C in 100% humidity and 5% CO_2 for up to 10 days in vitro.

Cell Viability Assay: Cell viability was assessed using a LIVE/DEAD Assay Kit (Invitrogen). Briefly, culture medium was replaced with Dulbecco's phosphate-buffered saline (DPBS; Invitrogen) containing calcein AM (4 μM) and ethidium homodimer-1 (2 μM). After 30 min incubation at 37 °C, the cells were changed into fresh culture media, and viewed under a fluorescence microscope (Leica DM IL; Leica Microsystems, Wetzlar, Germany) equipped with a digital camera (Leica DFC340 FX). Fluorescence images were acquired by excitation at 470 nm ± 20 nm and emission at 525 ± 25 nm for live cells, and excitation at 560 nm ± 20 nm and emission at 645 nm ± 40 nm for dead cells. Images were analyzed using NIH ImageJ software. Particles of positive staining with sizes between 10 and 50 μm were counted as individual cells, whereas those with sizes above 100 μm were counted as clusters. "Live growth area fraction", "Dead cell count per image" and "Live cell cluster size" were determined as the area with positive live staining divided by the total area of the image, the number of particles of positive dead staining divided by total number of particles, and the area of a cluster with positive live staining, respectively.

Immunostaining of Cells: Cells were fixed with 4% paraformaldehyde (Fisher Scientific, Pittsburgh, PA, USA) for 20 min, washed, permeablized with 0.1% Triton X-100 (Fisher Scientific) including 4% goat serum (Sigma) for 20 min, followed with incubation of primary antibodies overnight at 4 °C. After three 10 min washes, cells were incubated with secondary antibodies for 1 h at room temperature, followed with extensive washes. Mouse monoclonal anti-βIII-tubulin (b3TB, 1:1000; Sigma), rabbit polyclonal anti-glial fibrillary acidic protein (GFAP, 1:500; Sigma), and goat anti-mouse Alexa 488 and 568 (1:250; Invitrogen) secondary antibodies were used.

Statistical Analysis: Statistical differences were determined using a Mann-Whitney U test (Independent t-test, SPSS). Statistical significance was assigned as $*p < 0.05$, $**p < 0.01$ and $***p < 0.001$, respectively.

Supporting Information

Supporting Information is available from the Wiley Online Library or from the author.

Acknowledgements

The authors thank the NIH (AR005593, P41 EB002520, EB014283), the Air Force Office of Scientific Research, DARPA (W911NF-11-1-0079), and AFIRM for support of this research. A.S.W. acknowledges grants support from the Australian Research Council, the National Health and Medical Research Council and the Defense Health Foundation.

Received: September 16, 2012
Published online: March 8, 2013

[1] C. E. Schmidt, J. B. Leach, *Annu. Rev. Biomed. Eng.* **2003**, *5*, 293.
[2] A. Subramanian, U. M. Krishnan, S. Sethuraman, *J. Biomed. Sci.* **2009**, *16*, 108.
[3] X. Hu, X. Wang, J. Rnjak, A. S. Weiss, D. L. Kaplan, *Biomaterials* **2010**, *31*, 8121.
[4] X. Hu, S. H. Park, E. S. Gil, X. X. Xia, A. S. Weiss, D. L. Kaplan, *Biomaterials* **2011**, *32*, 8979.
[5] V. B. Rhovski, A. S. Weiss, *Eur. J. Biochem.* **1998**, *258*, 1.
[6] S. G. Wise, S. M. Mithieux, A. S. Weiss, *Adv. Protein Chem. Struct. Biol.* **2009**, *78*, 1.
[7] J. F. Almine, D. V. Bax, S. M. Mithieux, L. Nivison-Smith, J. Rnjak, A. Waterhouse, S. G. Wise, A. S. Weiss, *Chem. Soc. Rev.* **2010**, *39*, 3371.
[8] D. V. Bax, U. R. Rodgers, M. M. Bilek, A. S. Weiss, *J. Biol. Chem.* **2009**, *284*, 28616.
[9] D. W. Urry, *J. Phys. Chem. B* **1997**, *101*, 11007.
[10] F. G. Omenetto, D. L. Kaplan, *Science* **2010**, *329*, 528.
[11] Z. Shao, F. Vollrath, *Nature* **2002**, *418*, 741.
[12] H. J. Jin, D. L. Kaplan, *Nature* **2003**, *424*, 1057.
[13] X. Hu, K. Shmelev, L. Sun, E. S. Gil, S. H. Park, P. Cebe, D. L. Kaplan, *Biomacromolecules* **2011**, *12*, 1686.
[14] U. J. Kim, J. Park, H. J. Kim, M. Wada, D. L. Kaplan, *Biomaterials* **2005**, *26*, 2775.
[15] A. S. Lammel, X. Hu, S. H. Park, D. L. Kaplan, T. R. Scheibel, *Biomaterials* **2010**, *31*, 4583.
[16] X. Hu, Q. Lu, L. Sun, P. Cebe, X. Wang, X. Zhang, D. L. Kaplan, *Biomacromolecules* **2010**, *11*, 3178.
[17] M. E. Kinahan, E. Filippidi, S. Koster, X. Hu, H. M. Evans, T. Pfohl, D. L. Kaplan, J. Wong, *Biomacromolecules* **2011**, *12*, 1504.
[18] R. L. Horan, K. Antle, A. L. Collette, Y. Wang, J. Huang, J. E. Moreau, V. Volloch, D. L. Kaplan, G. H. Altman, *Biomaterials* **2005**, *26*, 3385.
[19] Y. Wang, H. J. Kim, G. Vunjak-Novakovic, D. L. Kaplan, *Biomaterials* **2006**, *27*, 6064.
[20] F. G. Omenetto, D. L. Kaplan, *Nat. Photonics* **2008**, *2*, 641.
[21] L. Yu, X. Hu, D. Kaplan, P. Cebe, *Biomacromolecules* **2010**, *11*, 2766.
[22] E. Bini, D. P. Knight, D. L. Kaplan, *J. Mol. Biol.* **2004**, *335*, 27.
[23] P. F. C. Wong, E. Bini, J. Huang, S. Y. Lee, D. L. Kaplan, *Appl. Phys. A-Mater.* **2006**, *82*, 223.
[24] G. Qin, S. Lapidot, K. Numata, X. Hu, S. Meirovitch, M. Dekel, I. Podoler, O. Shoseyov, D. L. Kaplan, *Biomacromolecules* **2009**, *10*, 3227.
[25] N. Annabi, S. M. Mithieux, A. S. Weiss, F. Dehghani, *Biomaterials* **2010**, *31*, 1655.
[26] X. Hu, D. Kaplan, P. Cebe, *Macromolecules* **2006**, *39*, 6161.
[27] X. Hu, Q. Lu, D. L. Kaplan, P. Cebe, *Macromolecules* **2009**, *42*, 2079.
[28] W. B. Teng, J. Cappello, X. Y. Wu, *Biomacromolecules* **2009**, *10*, 3028.

[29] W. Hwang, B. H. Kim, R. Dandu, J. Cappello, H. Ghandehari, J. Seog, *Langmuir* **2009**, *25*, 12682.
[30] J. A. Gustafson, H. Ghandehari, *Adv. Drug Delivery Rev.* **2010**, *62*, 1509.
[31] C. Baldock, A. F. Oberhauser, L. Ma, D. Lammie, V. Siegler, S. M. Mithieux, Y. Tu, J. Y. H. Chow, F. Suleman, M. Malfois, S. Rogers, L. Guo, T. C. Irving, T. J. Wess, A. S. Weiss, *Proc. Natl. Acad. Sci. USA* **2011**, *108*, 4322.
[32] J. Reguera, A. Fahmi, P. Moriarty, A. Girotti, J. C. Rodriguez-Cabello, *J. Am. Chem. Soc.* **2004**, *126*, 13212.
[33] M. Pyda, X. Hu, P. Cebe, *Macromolecules* **2008**, *41*, 4786.
[34] S. Park, E. S. Gil, H. Shi, H. J. Kim, K. Lee, D. L. Kaplan, *Biomaterials* **2010**, *31*, 6162.
[35] P. Toonkool, D. G. Regan, P. W. Kuchel, M. B. Morris, A. S. Weiss, *J. Biol. Chem.* **2001**, *276*, 28042.
[36] S. G. Wise, S. M. Mithieux, M. J. Raftery, A. S. Weiss, *J. Struct. Biol.* **2005**, *149*, 273.
[37] B. D. Lawrence, F. Omenetto, K. Chui, D. L. Kaplan, *J. Mater. Sci.* **2008**, *43*, 6967.
[38] J. Holst, S. Watson, M. S. Lord, S. S. Eamegdool, D. V. Bax, L. B. Nivison-Smith, A. Kondyurin, L. Ma, A. F. Oberhauser, A. S. Weiss, J. E. Rasko, *Nat. Biotechnol.* **2010**, *28*, 1123.
[39] B. F. Liu, J. Ma, Q. Y. Xu, F. Z. Cui, *Colloids Surf. B* **2006**, *53*, 175.
[40] R. A. Green, N. H. Lovell, L. A. Poole-Warren, *Biomaterials* **2009**, *30*, 3637.
[41] G. Harauz, V. Ladizhansky, J. M. Boggs, *Biochemistry* **2009**, *48*, 8094.
[42] H. Nojehdehian, F. Moztarzadeh, H. Baharvand, N. Z. Mehrjerdi, H. Nazarian, M. Tahriri, *Int. J. Artif. Organs* **2010**, *33*, 721.
[43] S. Lakard, G. Herlem, A. Propper, A. Kastner, G. Michel, N. Valles-Villarreal, T. Gharbi, B. Fahys, *Bioelectrochemistry* **2004**, *62*, 19.
[44] C. D. McCaig, A. M. Rajnicek, B. Song, M. Zhao, *Physiol. Rev.* **2005**, *85*, 943.